

Hadron yield correlation and constituent quark degree of freedom in heavy ion collisions

Rui-qin Wang,¹ Feng-lan Shao,^{1,*} Jun Song,² and Qu-bing Xie²

¹*Department of Physics, Qufu Normal University, Shandong 273165, People's Republic of China*

²*Department of Physics, Shandong University, Shandong 250100, People's Republic of China*

Based on the assumption of the production of deconfined quark matter, we use a quark combination model to systematically investigate hadron yields in heavy ion collisions from RHIC $\sqrt{s_{NN}} = 200, 130, 62.4$ GeV to SPS $E_{beam} = 158, 80, 40, 30, 20$ AGeV. We find that as the collision energy is greater than or equal to 30 AGeV the yields of various hadrons, their correlations, in particular, the observables $A = \frac{\bar{\Lambda} k^- p}{\Lambda k^+ \bar{p}}$ and $B = \frac{\Lambda k^- \Xi^+}{\Lambda k^+ \Xi^-}$, are all reproduced; however, as the collision energy drops to 20 AGeV quark combination fails. This indicates that the constituent quark degrees of freedom represent a decisive factor in thermal hadron production above 30 AGeV and seem to be invalid at 20 AGeV. In addition, hadron yields as well as particle ratios at midrapidity in the most central Pb+Pb collisions at $\sqrt{s_{NN}} = 5.5$ TeV are predicted.

PACS numbers: 25.75.Dw, 25.75.Gz, 25.75.Nq, 25.75.-q

I. INTRODUCTION

The question at which collision energy in heavy ion collisions the deconfinement is first reached has attracted more and more attentions in recent years [1–8]. The Beam Energy Scan programme of NA49 experiment at the CERN-SPS has suggested a preliminary answer — around 30 AGeV[9]. The ongoing Beam Energy Scan programme of STAR Collaboration at Brookhaven National Lab provides an opportunity to study it in more detail[10, 11]. Once the deconfined hot and dense quark matter is produced in heavy ion collisions, the observables of various thermal hadrons after hadronization, e.g. yields and momentum spectra etc, have some correlations originated from early quark degrees of freedom. One of the most typical examples is the elliptic flow (v_2) of hadrons measured at RHIC energies. As both v_2 and transverse momentum(p_T) are divided by the constituent quark number of hadron, the rescaled v_2 of various baryons and mesons, which are just that of constituent quarks, almost coincide with each other in the intermediate p_T range [12]. If the hot and dense quark matter is hadronized by quark (re-)combination/coalescence[13–15], as is commonly accepted, these correlations of hadrons can be beautifully explained. In quark (re-)combination/coalescence scenario, quarks and antiquarks are available in unbound state before hadronization and they can coalesce freely into various hadrons, and thereby these correlations from early quark degrees of freedom among different hadron species are naturally formed. On the other hand, if the deconfined quark matter is not produced at all in collisions, there is no free quarks and antiquarks (much less their subsequent combination) and these so-called “quark-level” correlations of hadrons maybe disappear or contort. Therefore, we can study whether the deconfinement is achieved by investigating these correlations among various hadrons produced in heavy ion collisions.

Hadron yield is one of the most significant observables from which one can obtain a lot of important information on the hot nuclear matter produced at the early stage of relativistic heavy ion collisions. At the high collision energies RHIC and top SPS, the yields of different hadron species have shown an explicit “quark-level” correlation in quark (re-)combination/coalescence scenario [15–17]. In this paper, we make an energy scan from RHIC energies $\sqrt{s_{NN}} = 200, 130, 62.4$ GeV to SPS energies $E_{beam} = 158, 80, 40, 30, 20$ AGeV to study at which collision energy this “quark-level” correlation of hadron yields first breaks. In particular, we define two correlation quantities $A = \frac{\bar{\Lambda} k^- p}{\Lambda k^+ \bar{p}}$ and $B = \frac{\Lambda k^- \Xi^+}{\Lambda k^+ \Xi^-}$, sensitive to quark degrees of freedom. The values of A and B are equal to one in the framework of quark (re-)combination/coalesce, independent of models. The deviation of A and B from one or not can be regarded as a possible signal of deconfinement in heavy ion collisions. We apply a quark combination model, which can exclusively describe hadron production and well reproduce the yields and momentum spectra of final-state hadrons in relativistic heavy ion collisions[18–23], to carry out the concrete calculations.

The paper is organized as follows. In Sec.II, we present the relations among yields of various hadrons in quark (re-)combination/coalescence scenario. In Sec.III, we use the quark combination model to calculate the yields of various hadrons, their yield ratios and correlation quantities $A = \frac{\bar{\Lambda} k^- p}{\Lambda k^+ \bar{p}}$ and $B = \frac{\Lambda k^- \Xi^+}{\Lambda k^+ \Xi^-}$ at midrapidity in the most central A+A collisions at different energies. Sec.IV summaries our work.

II. HADRON YIELDS IN QUARK (RE-)COMBINATION/COALESCENCE SCENARIO

Let us start from the general inclusive formula of hadron production in quark (re-)combination/coalescence

*Electronic address: shaofl@mail.sdu.edu.cn

scenario

$$N_M = \int dp_1 dp_2 F_{q\bar{q}}(p_1, p_2) \mathcal{R}_M(p_1, p_2) \quad (1)$$

$$N_B = \int dp_1 dp_2 dp_3 F_{qqq}(p_1, p_2, p_3) \mathcal{R}_B(p_1, p_2, p_3) \quad (2)$$

Here $F_{q\bar{q}}$ (F_{qqq}) is the joint quark-antiquark (three quark) distribution. \mathcal{R}_M (\mathcal{R}_B) is the combination function which stands for the formation probability of quark antiquark (three quarks) into a meson (baryon), dominated by chromodynamics. In sudden approximation, it is equal to the overlap between two (three) quark wave functions and the wave function of meson (baryon). Neglecting exotic (multi-quark) states, mesons and baryons exhaust all fate of quarks and antiquarks. One reaches the following relations: $\sum N_M + 3 \sum N_B = \sum N_q$ and $\sum N_M + 3 \sum N_B = \sum N_{\bar{q}}$, where N_q ($N_{\bar{q}}$) is the quark (antiquark) number of flavor q (\bar{q}). Extracting N_q and $N_{\bar{q}}$ from the joint two (three) quark distribution $F_{q\bar{q}}$ (F_{qqq}) and putting them out of the integral, one has the following schematic relations between hadron yields and quark numbers after integrating over quark momenta

$$N_{M(q\bar{q})} \propto C_M N_q N_{\bar{q}}, \quad N_{B(qqq)} \propto C_B N_q N_q N_q, \quad (3)$$

and quark number conservation will fix the proportionality coefficient. The effects of combination function on hadron yields are characterized with the factors C_M and C_B , and $C_M = C_{\bar{M}}$ and $C_B = C_{\bar{B}}$ are assumed.

One realized method of quark number conservation during combination is adding a factor b_q for each quark flavor in above equations, as did in ALCOR model [24],

$$N_{M(q\bar{q})} = C_M (b_q N_q) (b_{\bar{q}} N_{\bar{q}}), \quad (4)$$

$$N_{B(qqq)} = C_B (b_q N_q) (b_q N_q) (b_q N_q). \quad (5)$$

Then b_q can be uniquely determined by quark number conservation. According to Eqs.(4) and (5), we have the following relations between hadrons and the corresponding antihadrons

$$\begin{aligned} \frac{\bar{p}}{p} &= \left(\frac{b_{\bar{q}} \bar{q}}{b_q q}\right)^3, & \frac{k^+}{k^-} &= \left(\frac{b_q q}{b_{\bar{q}} \bar{q}}\right) \left(\frac{b_s \bar{s}}{b_s s}\right), \\ \frac{\bar{\Lambda}}{\Lambda} &= \left(\frac{b_{\bar{q}} \bar{q}}{b_q q}\right)^2 \frac{b_s \bar{s}}{b_s s}, & \frac{\Xi^-}{\Xi^+} &= \left(\frac{b_s s}{b_s \bar{s}}\right)^2 \frac{b_q q}{b_{\bar{q}} \bar{q}}. \end{aligned}$$

Here, we use particle symbols stand for their numbers for short, q for light quark number and s for strange quark number. Hiding the quark content in hadron yield, we obtain the following interesting relations among different hadron species

$$\frac{\bar{\Lambda} k^-}{\Lambda k^+} = \frac{\bar{p}}{p}, \quad \frac{\Lambda k^-}{\Lambda k^+} = \frac{\Xi^-}{\Xi^+}.$$

We define correlation quantities A and B as follows

$$A = \frac{\bar{\Lambda} k^- p}{\Lambda k^+ \bar{p}}, \quad B = \frac{\Lambda k^- \Xi^+}{\Lambda k^+ \Xi^-}. \quad (6)$$

If the quark matter exists and hadronizes via sudden (re-)combination/coalesce in heavy ion collisions, A and B should be equal to one for directly produced hadrons. It is a general result under the constraint of quark number conservation, which is independent of specific models.

Different from the well-known recombination and coalescence models [13, 14], the quark combination model [15, 25] is unique for its combination rule. The main idea of the combination rule is to line up the (anti)quarks in a one-dimensional order in phase space, e.g., in rapidity, and then let them combine into initial hadrons one by one according to this order[15]. Three (anti)quarks or a quark-antiquark pair in the neighborhood form a (anti)baryon or a meson, respectively. At last all quarks and antiquarks are combined into hadrons. The relations between hadron yields and the corresponding quark numbers are easily obtained [19]. With this rule, the model can give the yields and momentum distributions of all hadrons (included in the model) in an event, possessing some exclusive nature. The decay of the short-life resonances is systematically taken into account in the model. The model has been realized in Monte Carlo program and has described many properties of hadron production in relativistic heavy ion collisions [18–23].

III. RESULTS AND DISCUSSIONS

In this section, we use the quark combination model to calculate the hadron yields and their ratios as well as correlation quantities $A = \frac{\bar{\Lambda} k^- p}{\Lambda k^+ \bar{p}}$ and $B = \frac{\Lambda k^- \Xi^+}{\Lambda k^+ \Xi^-}$ at midrapidity in the most central A+A collisions at $\sqrt{s_{NN}} = 200, 130, 62.4$ GeV and $E_{beam} = 158, 80, 40, 30, 20$ AGeV. The predictions at LHC are also presented. The necessary input of the model, i.e., quark distribution just before hadronization, can be obtained by applying the hydrodynamics to describe the evolution of hot and dense quark matter just before hadronization, see Appendix A for details.

A. Hadron yields, their ratios and correlation quantities A and B

Table I shows the hadron density dN/dy at midrapidity in the most central A+A collisions at RHIC energies 200, 130, 62.4 GeV and SPS energies 158, 80, 40, 30, 20 AGeV. The experimental data are taken from Refs[9, 28–38]. The agreement between the calculation results and the experimental data is good except at 20 AGeV where χ^2/ndf is far greater than one. We note that ALCOR model [24] can also describe well the hadron yields at top SPS energy, which gives a cross-verification of quark combination. On the contrary, HIJING or HIJING/B model which is in compliance with the hadronic scenario for the early evolution of heavy ion collisions via a fragmentation hadronization, can not self-consistently explain the data of multi-strange hadrons [39, 40].

TABLE I: The calculated hadron yields dN/dy at midrapidity in the most central A+A collisions at different energies. The experimental data are taken from Refs[9, 28–38].

	Au+Au 200 GeV		Au+Au 130 GeV		Au+Au 62.4 GeV		Pb+Pb 158 AGeV	
	data	model	data	model	data	model	data	model
π^+	286.4 ± 24.2	281.0	$276 \pm 3 \pm 35.9$	267.2	233 ± 17	227.4	$170.1 \pm 0.7 \pm 9$	165.1
π^-	281.8 ± 22.8	281.8	$270 \pm 3.5 \pm 35.1$	270.5	237 ± 17	233.5	$175.4 \pm 0.7 \pm 9$	176.5
k^+	48.9 ± 6.3	48.6	$46.7 \pm 1.5 \pm 7.0$	45.2	37.6 ± 2.7	38.3	$29.6 \pm 0.3 \pm 1.5$	27.2
k^-	45.7 ± 5.2	46.1	$40.5 \pm 2.3 \pm 6.1$	42.4	32.4 ± 2.3	32.2	$16.8 \pm 0.2 \pm 0.8$	16.2
p	18.4 ± 2.6	17.0	$28.7 \pm 0.9 \pm 4.0$	25.7	29.0 ± 3.8	29.1	$29.6 \pm 0.9 \pm 2.9$	30.1
\bar{p}	13.5 ± 1.8	12.5	$20.1 \pm 1.0 \pm 2.8$	18.2	13.6 ± 1.7	13.5	$1.66 \pm 0.17 \pm 0.16$	1.91
Λ	$16.7 \pm 0.2 \pm 1.1$	15.3	$17.3 \pm 1.8 \pm 2.8$	14.5	$14.9 \pm 0.2 \pm 1.49$	13.7	$10.9 \pm 1.0 \pm 1.3$	13.3
$\bar{\Lambda}$	$12.7 \pm 0.2 \pm 0.9$	12.1	$12.7 \pm 1.8 \pm 2.0$	10.9	$8.02 \pm 0.11 \pm 0.8$	7.28	$1.62 \pm 0.16 \pm 0.2$	1.66
Ξ^-	$2.17 \pm 0.06 \pm 0.19$	2.05	$2.04 \pm 0.14 \pm 0.2$	1.93	$1.64 \pm 0.03 \pm 0.014$	1.67	$1.44 \pm 0.10 \pm 0.15$	1.18
$\bar{\Xi}^+$	$1.83 \pm 0.05 \pm 0.20$	1.69	$1.74 \pm 0.12 \pm 0.17$	1.53	$0.989 \pm 0.057 \pm 0.057$	1.02	$0.31 \pm 0.03 \pm 0.03$	0.23
Ω^-	$0.53 \pm 0.04 \pm 0.04$	0.56	$0.56 \pm 0.11 \pm 0.06$	0.52	$0.356 \pm 0.046 \pm 0.014$	0.379	$0.14 \pm 0.03 \pm 0.01$	0.11
$\bar{\Omega}^+$							$0.07 \pm 0.02 \pm 0.01$	0.04
χ^2/ndf	2.8/8		2.0/8		2.1/8		8.5/9	
	Pb+Pb 80 AGeV		Pb+Pb 40 AGeV		Pb+Pb 30 AGeV		Pb+Pb 20 AGeV	
	data	model	data	model	data	model	data	model
π^+	$132.0 \pm 0.5 \pm 7$	129.9	$96.6 \pm 0.4 \pm 6$	97.8	$83.0 \pm 0.4 \pm 4.2$	84.8	$72.9 \pm 0.3 \pm 3.6$	73.6
π^-	$140.4 \pm 0.5 \pm 7$	141.8	$106.1 \pm 0.4 \pm 6$	110.1	$96.5 \pm 0.5 \pm 4.8$	99.3	$84.8 \pm 0.4 \pm 4.2$	85.0
k^+	$24.6 \pm 0.2 \pm 1.2$	23.8	$20.1 \pm 0.3 \pm 1.0$	19.4	$21.2 \pm 0.8^{+1.5}_{-0.9}$	21.6	$16.4 \pm 0.6 \pm 0.4$	16.6
k^-	$11.7 \pm 0.1 \pm 0.6$	11.9	$7.58 \pm 0.12 \pm 0.4$	7.27	$7.8 \pm 0.1 \pm 0.2$	7.3	$5.58 \pm 0.07 \pm 0.11$	5.01
p	$30.1 \pm 1.0 \pm 3.0$	31.5	$41.3 \pm 1.1 \pm 4.1$	38.6	$42.1 \pm 2.0 \pm 4.2$	37.7	$46.1 \pm 2.1 \pm 4.6$	37.0
\bar{p}	$0.87 \pm 0.07 \pm 0.09$	0.83	$0.32 \pm 0.03 \pm 0.03$	0.36	$0.16 \pm 0.02 \pm 0.02$	0.17	$0.06 \pm 0.01 \pm 0.006$	0.07
Λ	$13.5 \pm 0.7 \pm 1.0$	14.5	$15.3 \pm 0.6 \pm 1.0$	14.7	$14.7 \pm 0.2 \pm 1.2$	14.2	$13.4 \pm 0.1 \pm 1.1$	11.5
$\bar{\Lambda}$	$1.06 \pm 0.08 \pm 0.1$	0.95	$0.42 \pm 0.04 \pm 0.04$	0.49	$0.21 \pm 0.02 \pm 0.02$	0.20	$0.10 \pm 0.02 \pm 0.01$	0.08
Ξ^-	$1.22 \pm 0.14 \pm 0.13$	1.23	$1.15 \pm 0.11 \pm 0.13$	1.10	$1.17 \pm 0.13 \pm 0.13$	1.38	$0.93 \pm 0.13 \pm 0.10$	0.92
$\bar{\Xi}^+$	$0.21 \pm 0.03 \pm 0.02$	0.15	$0.07 \pm 0.01 \pm 0.01$	0.08	$0.05 \pm 0.01 \pm 0.01$	0.07	-----	0.02
$\Omega^- + \bar{\Omega}^+$	-----	0.13	$0.10 \pm 0.02 \pm 0.02$	0.09	-----	0.14	-----	0.07
χ^2/ndf	2.9/7		3.0/8		5.6/7		15.3/6	

Fig. 1 shows the ratios of antihadrons to hadrons at midrapidity as the function of collision energy. The filled triangles are the calculated results, and the experimental data are taken from Refs[9, 28–30, 32–34, 36–38]. These ratios are mainly influenced by the non-zero baryon number density. As the collision energy increases, the nuclear transparency power becomes strong and baryon number density at midrapidity becomes small. This results in a rapid increase for ratios of K^-/K^+ , \bar{p}/p , $\bar{\Lambda}/\Lambda$ with the increasing collision energy. π^-/π^+ follows a different pattern. At low collision energies π^-/π^+ is slightly higher than one, while it is close to one at high energies. This is caused by the asymmetry of decay contribution from hyperons and anti-hyperons (e.g. $\Lambda \rightarrow p\pi^-$). As the collision energy increases, the yields of hyperons are close to that of anti-hyperons and their decay contributions to pion yields are almost the same and therefore the ratio of π^-/π^+ is close to one.

Fig. 2 shows the ratios of baryons to mesons p/π and the strangeness ratios K/π at midrapidity as the function of collision energy. The filled triangles (up and down) are

the computed results, and the experimental data are taken from Refs[9, 28, 32–34, 36, 37]. The big splits between p/π^+ and \bar{p}/π^- and between K^+/π^+ and K^-/π^- at low collision energies is due to the high baryon number density. At 20 AGeV, the result of p/π^+ deviates seriously from the data. This is probably because the participant nucleons are not broken completely in collisions. These nucleon fragments deposited in midrapidity region lead to the extra contribution of proton production besides those from quark combination and lead to the excessively high ratio of p/π^+ .

Following the experimental data in Table I, A and B at different collision energies are evaluated and the results are presented with squares in Fig. 3. We find that the data of A and B at RHIC energies are almost equal to one while at SPS energies they deviate from one; particularly, at 20 AGeV the value of A amounts to two, seriously deviating from one (the data for B are unavailable). This is probably because the decay of resonances will blur A and B to a certain degree. In order to explore the decay effect, we use the quark combination model to compute the values

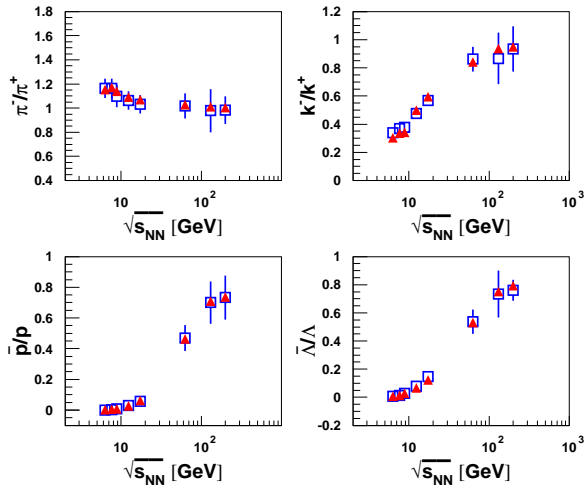


FIG. 1: (Color online) The yield ratios of antihadrons to hadrons at midrapidity as the function of the collision energy. The filled symbols are the calculated results, and the experimental data, open symbols with error bar, are from Refs[9, 28–30, 32–34, 36–38].

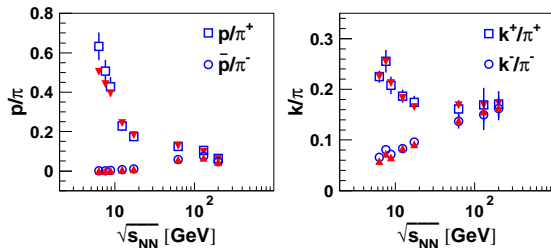


FIG. 2: (Color online) The values of the relative production yields p/π and k/π at different energies. The triangles down are the numerical results for p/π^+ and k^+/π^+ , and the triangles up are the numerical results for \bar{p}/π^- and k^-/π^- . The experimental data, open symbols with error bar, are from Refs[9, 28, 32–34, 36, 37].

of A and B for the directly produced hadrons and the final-state hadrons, respectively. The dashed lines are the results of directly produced hadrons. Just as analyzed above, the dashed lines keep an invariant value of one for both A and B, independent of collision energy. The very small fluctuations of dashed lines are due to the fact that the rapidity distributions of the formed hadrons are slightly different from those of quarks, which leads to a small amount of hadrons formed by midrapidity quarks escape from the midrapidity region [18]. The filled triangles down are model results of final-state hadrons. We see that as collision energy is greater than 30 AGeV these triangles agree well with the experimental data within statistical uncertainties. Removing the part of resonance decay, the data of A and B for directly produced hadrons should be equal to one, respectively. This suggests the existence of the “quark level” correlation of directly produced hadrons at these collision

energies. However, at 20 AGeV the value of A calculated via quark combination for final state hadrons seriously deviates the data. This in itself indicates the quark degrees of freedom do not represent a decisive factor in hadron production at 20 AGeV.

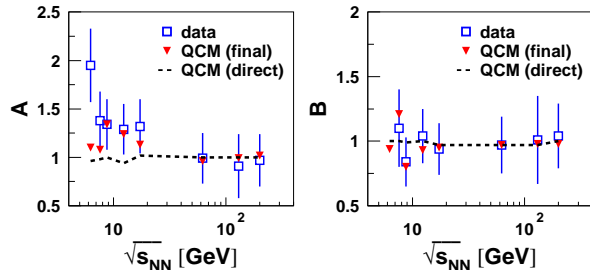


FIG. 3: (Color online) The correlation quantities A and B as the function of collision energy. The experimental data, open symbols with error bar, are from Refs[9, 28–30, 32–38].

From the above analysis of hadron yields, hadron ratios and correlation quantities A and B, we find that as the collision energy is greater than or equal to 30 AGeV the quark combination can describe reasonably well all these observables which indicates the existence of constituent quark degrees of freedom in the energy region. When the collision energy drops to 20 AGeV, however, the quark combination mechanism can not self-consistently describe these quantities, in particular the correlation quantity A. Note that in order to best fit the data of hadron yields, we have adjusted the strangeness parameter λ_s (see Table IV) to the quite high values at 20, 30 AGeV which are far greater than the saturated values at higher collision energies and are also greater than those at lower collision energies [41]. But even so the quark combination can not self-consistently explain the data at 20 AGeV. In addition, the high strangeness entangled with baryon density leads to the Sawtooth-like shape for calculated final-state A and B at low SPS energies. In fact this peak behavior of strangeness (i.e. K^+/π^+ ratio or λ_s determined mainly by the former) at low SPS energies has been interpreted in Ref [2, 4] as a result of onset of deconfinement, i.e. the result of strangeness carrier changing from strange hadrons to strange quarks at the onset of deconfinement. The failure of quark combination energy indicates the (partial) disappearance of constituent quark degrees of freedom and closely relates to the onset of deconfinement around 30 AGeV observed by NA49 Collaboration [9].

B. Predictions at LHC

With the increasing collision energy, the strangeness λ_s of the hot and dense quark matter in Table IV tends to be saturated and the squared sound velocity c_s^2 approaches an ideal value 1/3 and the baryon number density n_0 decreases regularly. So we take $\lambda_s=0.43$, $c_s^2 = 1/3$ and $n_0 = 0.0 fm^{-3}$ at $\sqrt{s_{NN}} = 5.5$ TeV. The initial entropy den-

sity of the central point at the beginning of hydrodynamic evolution is taken to be $256.5/\text{fm}^3$ according to Eq. (A7). In Tables II and III, we present our predictions of hadron yields and hadron ratios at LHC energy ($\sqrt{s_{NN}} = 5.5$ TeV). Our computed particle ratios are consistent with the results of the thermal model in Ref[7].

TABLE II: The predicted dN/dy of identified hadrons at midrapidity in the most central (0 – 5%) Pb+Pb collisions at $\sqrt{s_{NN}} = 5.5$ TeV.

π^+	π^-	k^+	k^-	p	\bar{p}	Λ	$\bar{\Lambda}$	Ξ^-	Ξ^+	Ω^-	Ω^+
435.5	435.5	71.6	71.6	34.6	34.6	20.5	20.5	2.9	2.9	0.4	0.4

TABLE III: The predicted hadron ratios at midrapidity in the most central Pb+Pb collisions at $\sqrt{s_{NN}} = 5.5$ TeV.

p/π^+	\bar{p}/π^-	k^+/π^+	k^-/π^-	Λ/π^-	Ξ^-/π^-	Ω^-/π^-
0.079	0.079	0.165	0.165	0.047	0.007	0.001

IV. SUMMARY

In this paper, we used the quark combination model to make a systematical study of the hadron yields in heavy ion collision in a broad collision energy region. At the collision energies where the deconfined quark matter has been created, the yields of various hadrons after hadronization have some correlations inherited from the early quark degrees of freedom. We investigate at which collision energy this “quark-level” correlation of hadron yields first breaks. We apply the hydrodynamics to describe the evolution of deconfined quark matter and to obtain the quark distribution just before hadronization, then utilize the quark combination model to describe hadronization. We find that as the collision energy is greater than or equal to 30 AGeV, the quark combination well reproduce the yields of various hadrons, their ratios and correlation quantities A and B; however, as the collision energy drops to 20 AGeV, the mechanism can not self-consistently describe these quantities. This indicates that the constituent quark degrees of freedom represent a decisive factor in thermal hadron production above 30 AGeV and seem to be invalid at 20 AGeV. It is related to the onset of deconfinement observed at collision energy 20-30 AGeV. Finally, we predict the yields of various hadrons and their ratios in the most central Pb+Pb collisions at $\sqrt{s_{NN}} = 5.5$ TeV.

ACKNOWLEDGMENTS

The authors thank Z. T. Liang, Q. Wang and G. Li for helpful discussions. R. Q. Wang would like to thank L. G. Pang and J. Deng for fruitful discussions. The work is

supported in part by the National Natural Science Foundation of China under the grant 10775089, 10947007 and 10975092.

Appendix A: Quark distribution just before hadronization

The quark distribution just before hadronization is needed for the quark combination to describe the hadron production in relativistic heavy ion collisions. Here, we use relativistic hydrodynamics [43–45] to describe the time-space evolution of the hot and dense quark matter before hadronization. The evolution equation of hydrodynamics follows from the local conservation laws for energy, momentum, and other conserved charges, e.g. baryon number,

$$\partial_\mu T^{\mu\nu}(x) = 0, \quad (\nu = 0, 1, 2, 3) \quad (\text{A1})$$

$$\partial_\mu j^\mu(x) = 0, \quad (\text{A2})$$

by inserting the ideal fluid decomposition

$$T^{\mu\nu}(x) = (e(x) + p(x))u^\mu(x)u^\nu(x) - g^{\mu\nu}p(x), \quad (\text{A3})$$

$$j^\mu(x) = n(x)u^\mu(x). \quad (\text{A4})$$

Here, $u^\mu(x) = \gamma(1, v_x, v_y, v_z)$ with $\gamma = 1/\sqrt{1 - v_x^2 - v_y^2 - v_z^2}$ is the local four velocity of a thermalized fluid cell; $e(x)$ is the energy density, $p(x)$ the pressure, and $n(x)$ the conserved number density.

As the energy density of the fluid cell drops to 1.0 GeV/fm³ (a common criteria of phase transition from Lattice QCD[46]), we stop the hydrodynamic evolution and let the constituent quarks and antiquarks freeze out according to Cooper-Frye formalism [47]

$$E \frac{dN_i}{d^3p} = \frac{dN_i}{dy p_T d p_T d\varphi} = \frac{g_i}{(2\pi)^3} \int_\Sigma f_i(p \cdot u(x), x) p \cdot d^3\sigma(x), \quad (\text{A5})$$

where $d^3\sigma(x)$ is the outward normal vector on the freeze-out surface $\Sigma(x)$, g_i the degeneracy factor of quarks ($g_i = 6$). The phase-space distribution f in the formula is taken to be a local equilibrium distribution,

$$f_i(E, x) = \frac{1}{\exp[(E - \mu_i(x))/T(x)] + 1}. \quad (\text{A6})$$

We consider only the freeze-out of light and strange quarks and antiquarks. The three chemical potentials $\mu_q, \mu_{\bar{q}}$ and $\mu_s = \mu_{\bar{s}}$ at freeze-out can be determined uniquely by the global conservation of energy and baryon number plus an ancillary constraint of strangeness.

We study in this paper the hadron production in midrapidity region only. The code of Kolb[48–50] for 2+1- dimensional hydrodynamics with the longitudinal boost invariance is used to simulate the evolution of quark system before hadronization.

TABLE IV: The values of the initial baryon density n_0 , strangeness factor λ_s and squared sound velocity c_s^2 in central A+A collisions at different energies.

Energy	200GeV	130GeV	62.4GeV	158AGeV	80AGeV	40AGeV	30AGeV	20AGeV
n_0 (fm^{-3})	0.30	0.34	0.74	1.31	1.46	1.64	1.74	1.56
λ_s	0.43	0.43	0.43	0.44	0.50	0.57	0.80	0.70
c_s^2	1/3.1	1/3.4	1/4.0	1/6.0	1/6.0	1/6.0	1/6.0	1/6.0

These frozen-out quarks and antiquarks with momentum distributions in Eq. (A5) are hadronized by the quark combination model[15, 25]. In this method of hydrodynamics + quark combination, the quark combination model is default setting while some inputs for hydrodynamics need fixing. The first is initial entropy density s_0 of the central point at the beginning of hydrodynamic evolution. The distribution of transverse entropy density is determined by optical Glauber model[26]. We apply the following empirical formula of s_0 [27] as the function of collision energy $\sqrt{s_{NN}}$

$$s_0(\sqrt{s_{NN}}) = 6.99 \times 10^{-3} (312.5 \log_{10} \sqrt{s_{NN}} - 64.8)^{3/2}. \quad (A7)$$

The second is the initial baryon number density n_0 at cen-

tral point fixed by the data of the net-proton rapidity density. The distribution of transverse baryon number density is also determined by optical Glauber model. The third is the equation of state $p = p(e)$ for the hot and dense quark matter which is taken to be the simplest pattern $p = c_s^2 e$. The squared sound velocity c_s^2 is obtained by fitting the data of transverse momentum spectra of protons. The fourth is the strangeness of hot and dense quark matter denoted by the factor $\lambda_s = 2\langle s\bar{s} \rangle / \langle u\bar{u} + d\bar{d} \rangle$. In order to make a better description of strange hadrons, we regard it as a free parameter in the present paper. The values of n_0 , λ_s and c_s^2 in central A+A collisions at different energies are shown in Table IV. We note that the extracted λ_s around 30 AGeV are quite high which are consistent with the analytic results of thermal model [41].

-
- [1] L. Van Hove, Phys. Lett. B **118**, 138 (1982).
[2] M. Gaździcki and D. Röhrich, Z. Phys. C **65**, 215 (1995); **71**, 55 (1996), and references therein.
[3] M. Gaździcki, Z. Phys. C **66**, 659 (1995).
[4] M. Gaździcki and M. I. Gorenstein, Acta Phys. Polon. **B 30**, 2705 (1999).
[5] M. I. Gorenstein, M. Gaździcki, and K. A. Bugaev, Phys. Lett. B **567**, 175 (2003).
[6] S. V. Akkelin and Yu. M. Sinyukov, Phys. Rev. C **73**, 034908 (2006).
[7] A. Andronic, P. Braun-Munzinger and J. Stachel, Phys. Lett. B **673**, 142(2009).
[8] S. Zhang, J. H. Chen, H. Crawford, D. Keane, Y. G. Ma and Z. B. Xu, arXiv:nucl-ex/0908.3357.
[9] C. Alt *et al.* (NA49 Collaboration), Phys. Rev. C **77** 024903 (2008).
[10] L. Kumar, J. Phys. G **36** 064066 (2009), and references therein.
[11] B. I. Abelev *et al.* STAR Note SN0493: <http://drupal.star.bnl.gov/STAR/starnotes/public/sn0493>.
[12] A. Adare, *et al.* (PHENIX Collaboration), Phys. Rev. Lett. **98**, 162301 (2007).
[13] R. J. Fries, B. Müller, C. Nonaka, and S. A. Bass, Phys. Rev. Lett. **90**, 202303 (2003).
[14] V. Greco, C. M. Ko, and P. Lévai, Phys. Rev. Lett. **90**, 202302 (2003).
[15] F. L. Shao, Q. B. Xie and Q. Wang, Phys. Rev. C **71**, 044903 (2005).
[16] A. Bialas, Phys. Lett. B **442**, 449(1998).
[17] J. Zimányi, T. S. Biró, T. Csörgő and P. Lévai, Phys. Lett. B **472** 243 (2000).
[18] F. L. Shao, T. Yao and Q. B. Xie, Phys. Rev. C **75**, 034904 (2007).
[19] C. E. Shao, J. Song, F. L. Shao and Q. B. Xie, Phys. Rev. C **80**, 014909 (2009).
[20] J. Song, F. L. Shao and Q. B. Xie, Int. J. Mod. Phys. A **24**, 1161(2009).
[21] D. M. Wei, F. L. Shao, J. Song and Y. F. Wang, Int. J. Mod. Phys. A **23**, 5217(2008).
[22] Y. F. Wang, F. L. Shao, J. Song, D. M. Wei and Q. B. Xie, Chin. Phys. C **32**, 976(2008).
[23] W. Han, S. Y. Li, Y. H. Shang, F. L. Shao and T. Yao, Phys. Rev. C **80**, 035202 (2009).
[24] T. S. Biró, P. Lévai and J. Zimányi, Phys. Lett. B **347** 6 (1995).
[25] Q. B. Xie and X. M. Liu, Phys. Rev. D **38**, 2169 (1988).
[26] R. J. Glauber, in“Lectures on T Physics” **1** (W. E. Brittin, L. G. Dunham eds., Interscience, NY, 1959).
[27] Gregory Kestin and Ulrich Heinz, arXiv:nucl-th/0806.4539.
[28] C. Alt *et al.* (NA49 Collaboration), Phys. Rev. C **73** 044910 (2006).
[29] C. Alt *et al.* (NA49 Collaboration), Phys. Rev. C **78** 034918 (2008).
[30] T. Anticic *et al.* (NA49 Collaboration), Phys. Rev. Lett. **93** 022302 (2004).
[31] C. Alt *et al.* (NA49 Collaboration), Phys. Rev. Lett. **94** 192301 (2005).
[32] S. V. Afanasiev *et al.* (NA49 Collaboration), Phys. Rev. C **66** 054902 (2002).
[33] B. I. Abelev *et al.* (STAR Collaboration), Phys. Rev. C **79** 034909 (2009).
[34] K. Adcox *et al.* (PHENIX Collaboration), Phys. Rev. Lett. **89** 092302 (2002).
[35] J. Adams *et al.* (STAR Collaboration), Phys. Rev. Lett. **92**

- 182301 (2004).
- [36] K. Adcox *et al.* (PHENIX Collaboration), Phys. Rev. C **69** 024904 (2004).
- [37] S. S. Adler *et al.* (PHENIX Collaboration), Phys. Rev. C **69** 034909 (2004).
- [38] J. Adams *et al.* (STAR Collaboration), Phys. Rev. Lett. **98** 062301 (2007).
- [39] V. Topor Pop, A. Andrighetto, M. Morando, F. Pellegrini, R. A. Ricci, G. Segato, arXiv:hep-ph/9407262 (1994).
- [40] P. Csizmadia, P. Lévai, S. E. Vance, T. S. Biró, M. Gyulassy and J. Zimányi, J. Phys. G: Nucl. Part. Phys. **25** 321 (1999).
- [41] P. Braun-Munzinger, K. Redlich and J. Stachel, arXiv:nucl-th/0304013 and references therein. Invited review in: R.C. Hwa, X.N. Wang (Eds.), Quark Gluon Plasma 3, World Scientific, Singapore, 2004.
- [42] A. Andronic, P. Braun-Munzinger, J. Stachel, Nucl. Phys. A **772** 167 (2006).
- [43] L. D. Landau, Izv. Akad. Nauk SSSR Ser. Fiz. **17** 51 (1953).
- [44] Dirk H. Rischke, Stefan Bernard and Joachim A. Maruhn, Nucl. Phys. A **595** 346 (1995).
- [45] Peter F. Kolb and Ulrich Heinz, arXiv:nucl-th/0305084. Invited review in: R.C. Hwa, X.N. Wang (Eds.), Quark Gluon Plasma 3, World Scientific, Singapore, 2004.
- [46] F. Karsch, Nucl. Phys. A **698**, 199 (2002).
- [47] F. Cooper and G. Frye, Phys. Rev. D **10** 186 (1974).
- [48] Peter F. Kolb, Josef Sollfrank and Ulrich Heinz, Phys. Rev. C **62**, 054909 (2000).
- [49] Peter F. Kolb, U. Heinz, P. Huovinen, K.J. Eskola, K. Tuominen, Nucl. Phys. A **696** 197 (2001).
- [50] Peter F. Kolb, and Ralf Rapp, Phys. Rev. C **67**, 044903 (2003).